JOURNAL OF SPACECRAFT AND ROCKETS
Vol. 31, No. 6, November–December 1994

Convective and Radiative Heat Transfer Analysis for the Fire II Forebody

Robert B. Greendyke*
ViGYAN, Inc., Hampton, Virginia 23666
and
Lin C. Hartung†
NASA Langley Research Center, Hampton, Virginia 23681

A Navier–Stokes flowfield solution method using finite-rate chemistry and two-temperature thermal nonequilibrium was used in combination with two nonequilibrium radiative heat transfer codes to calculate heating for the FIRE II vehicle. An axisymmetric model of the actual body shape was used. One radiative heating code was used in uncoupled fashion with the flowfield solver's energy equations, while the other code was used in both coupled and uncoupled variations. Several trajectory points ranging from highly nonequilibrium flow to near-equilibrium flow were used for a study of both convective and radiative heating over the vehicle. Considerable variation in radiative heating was seen at the extremes, while agreement was good in the intermediate trajectory points. Total heat transfer calculations gave good comparison until the peak heating trajectory points were encountered and returned to good agreement for the last two equilibrium points.

Nomenclature

a = thermal exponent used in Eq. (1), usually equal to 0.3, but redefined by Eq. (2)
b = thermal exponent used in Eq. (1), usually equal to 0.7, but redefined by Eq. (3)
e_λ = radiative emission coefficient, W/cm^3 − μ − sr
I^i_λ = specific radiative intensity at spatial point i, W/cm^3 − μ − sr
Q_R = incident radiative flux as defined in Eq. (7), W/cm^2
$Q^i_{R\lambda}$ = radiadive flux as a function of wavelength at spatial point i, W/cm^2 − μ
T_{ave} = average temperature defined by Eq. (1) K
T_e = electron temperature, K
T_H = heavy particle translational temperature, K
T_V = heavy particle vibrational temperature, K
z = gas layer thickness in direction normal to body surface, cm
α'_λ = radiative absorption coefficient corrected for stimulated emission, cm^{-1}

Subscripts

λ = wavelength, Å
σ_V = limiting vibrational excitation cross section, m^2
θ = solid angle, sr

Introduction

ONE technique for atmospheric re-entry and vehicle trajectory manipulation that may become available to future space vehicles is aerobraking. Aerobraking is an economical method that would use a heat shield to take advantage of aerodynamic drag in a pass through the Earth's, or another planet's, upper atmosphere. The resulting loss of momentum by frictional dissipation would permit entry into orbit, or a shift from one orbit to another. Unfortunately, the high altitudes and hypersonic speeds at which these vehicles will be operating represent a considerable challenge to existing computational methods for flowfield and heat transfer analysis. In particular, the calculation of nonequilibrium radiative heat transfer in this regime is the subject of considerable uncertainty. Considering that the radiative contribution to the overall heat transfer could be as high as 50% or more, accurate modeling of nonequilibrium radiative phenomena is vital to heat shield design. It is, therefore, important to compare the results from computational methods to results obtained from flight experiments.

Although several flight experiments, such as the Apollo 4[1] and the Planetary Atmosphere Experiments Test (PAET),[2] were flown in regimes similar to aerobraking flight regimes, the flight data from the FIRE experiment[3,4] were deemed the most appropriate for this study. The FIRE project was designed to provide data on the aerothermal environment surrounding a blunt body during reentry to Earth at a nominal velocity of 11.35 km/s. This project provided data that encompass flow regimes from high-altitude, high-velocity, largely nonequilibrium flows to relatively low-altitude, low-velocity, equilibrium flows.

Computational studies[5–7] of the aerothermal heating have already been conducted for the FIRE II experiment utilizing a variety of computational techniques. Sutton[5] used an inviscid chemical equilibrium approach with radiation coupled to the energy equation for equivalent spheres through the FIRE II's trajectory. Balakrishnan[6] used an equilibrium viscous shock-layer code with coupled equilibrium radiation in chemical and thermal equilibrium for equivalent sphere bodies. Gupta[7] studied the FIRE II trajectory with both equilibrium and nonequilibrium chemistry models and coupled equilibrium radiation models in Navier–Stokes and viscous shock layer codes. However, none of these studies used a state-of-the-art thermochemical nonequilibrium Navier–Stokes solution method combined with a nonequilibrium radiation solution method. This was done by Park[8] and Hartung et al.[9] for uncoupled equivalent sphere bodies for selected points from the early part of the FIRE II's trajectory well before the vehicle's peak heating point. Neither Park nor Hartung et al. used these methods throughout the vehicle's trajectory, or used the actual shape of the FIRE vehicle in their calculations. The present work is the first use of the actual body shape in FIRE II calculations.

The purpose of this investigation is to re-examine the FIRE II heat transfer data and to compare these with solutions obtained for the actual forebody by the langley upwind relaxation algorithm (LAURA) code,[10,11] a Navier–Stokes flowfield solution method us-

Received June 17, 1993; revision received Sept. 13, 1993; accepted for publication Oct. 21, 1993.

*Research Engineer. Member AIAA.
†Aerospace Engineer, Aerothermodynamics Branch, Space Systems Division. Member AIAA.

ing finite-rate chemistry in thermal and chemical nonequilibrium. The LAURA code was used in conjunction with nonequilibrium radiative heat transfer solutions calculated by two methods, the nonequilibrium air radiation (NEQAIR)[12] and the langley optimized radiative nonequilibrium (LORAN)[13] codes. The NEQAIR code was used in an uncoupled fashion, whereas the LORAN code provided both coupled and uncoupled results for information on the influence of radiative coupling. The study used the actual forebody shape of the FIRE vehicle and was conducted at selected trajectory points (Table 1) throughout the FIRE II's trajectory. This study represents follow-up research to a previous study by Gnoffo,[14] wherein the LAURA, NEQAIR, and LORAN codes were used to study the near equilibrium shock layer over a lunar transfer vehicle (LTV). As a side issue, the radiative structure of the calculated FIRE II shock layers was studied using the NEQAIR code in the same methodology as Greendyke.[15]

Flowfield Solution Method

The LAURA code[10,11] was the sole flowfield solution method used throughout this investigation for the determination of FIRE II flowfields and convective heat transfer rates. The LAURA code is a point-implicit relaxation algorithm for obtaining the numerical solution to the governing equations for viscous hypersonic flows in chemical and thermal nonequilibrium. The algorithm is derived using a finite-volume formulation in which the inviscid components of the flux across cell walls are described with Roe's averaging[16] and Harten's entropy fix[17] with a total variation diminishing scheme described by Weilmuenster and Gnoffo.[18] The code includes eleven species continuity equations, three momentum equations, and one energy equation each for both the vibrational–electronic and total energies. The vibrational and electronic energies of all species are assumed to be in equilibrium at a temperature T_V and the translational and rotational energies in equilibrium at temperature T_H. Given that the actual FIRE II heatshield was beryllium, a fully catalytic wall boundary condition was used for all the FIRE II flowfield calculations.

The effect of kinetic models on the calculation of radiative heat transfer was examined in a recent study,[19] and it was concluded that the most appropriate models are a reference value of the ionization potential that represents the energy required to ionize a molecule or atom from an already excited state. The chemical rates of Park[20] were used. In addition, Park's two-temperature model[8] for the rate controlling temperature T_{ave} was used:

$$T_{ave} = T_V^a \times T_H^b \tag{1}$$

where the exponents are, following the suggestion of Hansen,[21] replaced with

$$a = \left[0.1 + 0.4 * \left(\frac{T_V}{T_H}\right)\right] \tag{2}$$

and

$$b = 1.0 - \left[0.1 + 0.4 * \left(\frac{T_V}{T_H}\right)\right] \tag{3}$$

In addition, the species number density used in Eq. 56 of Ref. 11 was changed to the total number density to better reflect true collisional probabilities. The limiting cross section for vibrational excitation σ_V utilized Park's curve fit[8]:

$$\sigma_V = 1 * 10^{-17}\left(\frac{50{,}000}{T_H}\right)^2 \tag{4}$$

The axisymmetric solution grid utilized in all solutions had 64 cells in the direction normal to the body, and 30 cells along the surface of the body. A grid convergence study performed at the 1643 s trajectory point indicated that this grid would provide acceptable resolution for convective heat transfer analysis. The actual FIRE II forebody shape was used for all three heat shields, as described in Ref. 3. To facilitate convergence, grid adaption in the shock front[14] was utilized for the 1643–1652 s trajectory points, as can be seen when comparing Fig. 1 (with an nonadapted shock grid) to Fig. 2 (with grid adaption at the shock). Freestream conditions[7] are listed in Table 1.

Table 1 FIRE II trajectory points

Time, s	Altitude, km	Velocity, km/s	Density, kg/m^3	T_∞, K	T_W, K
1634.0	76.42	11.36	3.72×10^{-5}	195	615
1636.0	71.04	11.31	8.57×10^{-5}	210	810
1640.5	59.26	10.97	3.86×10^{-4}	254	1560
1643.0	53.04	10.48	7.80×10^{-4}	276	640
1645.0	48.37	9.83	1.32×10^{-3}	285	1520
1648.0	42.14	8.30	3.00×10^{-3}	267	1560
1651.0	37.19	6.19	6.05×10^{-3}	253	1060
1652.0	35.86	5.49	7.28×10^{-3}	252	1160

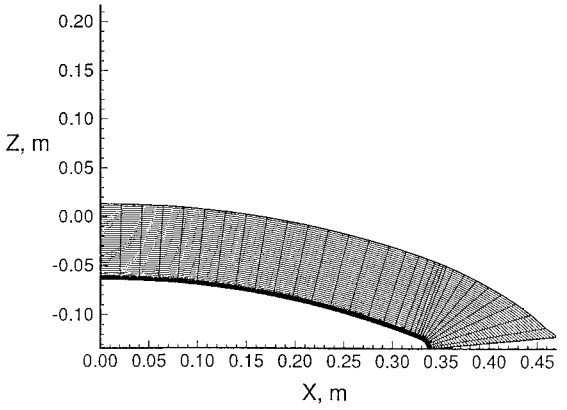

Fig. 1 Computational grid at 1634 s.

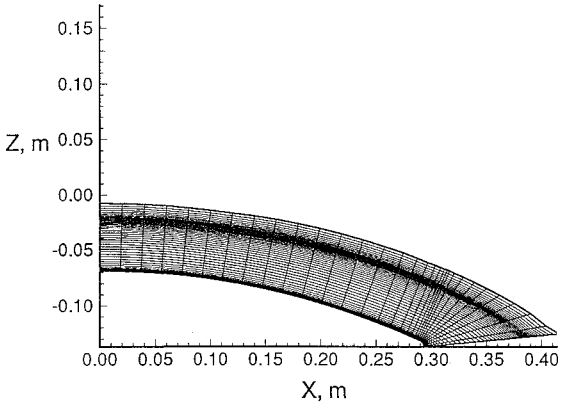

Fig. 2 Computational grid at 1652 s.

Nonequilibrium Radiation Solution Methods

The NEQAIR code was used to solve for the radiative heat transfer in an uncoupled fashion, while the LORAN code was used in both an uncoupled and coupled fashion with the LAURA code. Note that the three codes used in this paper were all originally developed without radiative coupling effects. In addition, the NEQAIR code was used to examine the radiative processes at some of the FIRE II trajectory points in the same fashion as a previous study of aerobrake shock-layer radiative processes.[15]

NEQAIR Code

The NEQAIR code calculates the population distribution of atoms and molecules among their states by use of a quasi-steady-state assumption (QSS).[8] The QSS assumes that the rate at which an electronic state is populated or depopulated greatly exceeds the difference between the two rates, and therefore, the difference can be ignored. With known population rates, the number densities of the electronic states can then be calculated by matrix inversion given the

known thermodynamic conditions at a local point in the flowfield. The NEQAIR code then calculates the radiative emission and absorption coefficients on a line-by-line basis over the spectral region specified.

For this investigation, the spectral region considered is between 800–15,000 Å. In a previous investigation,[14] spectral grid convergence difficulties were noticed using the NEQAIR code. To avoid this problem, the method used in that investigation is applied. First, the uv and vacuum uv region between 800–2000 Å is solved using 20,000 spectral grid point locations. The uv, visible, and IR regions are then solved between 2000 and 15,000 Å also using 20,000 points. After the completion of this study, calculations were done using the NEQAIR code at the peak radiative heating point using a spectral grid resolution of approximately 0.02 Å in the spectral region between 8000–12,000 Å. It was found that the increased resolution only changed the calculated flux to the wall by 1% at a substantial increase in computational effort. It is, therefore, believed that the spectral resolution of 20,000 points in the 2000–15,000 Å region was sufficiently accurate for this investigation.

The absorbing radiative flux is calculated by assuming that each grid point i constitutes a thermodynamically homogeneous layer. The radiative intensity, as a function of wavelength at each point, is then[22]

$$I_\lambda^{i+1} = \left(\frac{e_\lambda}{\alpha'_\lambda}\right) * \left(1 - e^{-\alpha'_\lambda z}\right) + I_\lambda^i e^{-\alpha'_\lambda z} \tag{5}$$

The radiative intensity at each spatial location of the flowfield can then be integrated over a 2π sr solid angle to obtain a thin gas, or $2\pi I$, approximation to the radiative flux as a function of wavelength $Q_{R\lambda}^{i+1}$. Or

$$Q_{R\lambda}^{i+1} = I_\lambda^{i+1} \int_0^{2\pi} \mathrm{d}\theta \tag{6}$$

in a marching fashion from the shock to the wall.

The total radiative heating Q_R is then found by integrating over the wavelength at the cell closest to the wall

$$Q_R = \int_{\lambda\,\min}^{\lambda\,\max} Q_{R\lambda}^{\mathrm{Wall}}\,\mathrm{d}\lambda \tag{7}$$

The incident radiative flux, as a function of wavelength, was retained at the cell closest to the wall. The flux information was then postprocessed to determine the contribution of radiative heating to the wall when the surface absorptance α is included. The surface absorptance of the beryllium heat shield was obtained from Ref. 3. Total heating to the wall from both convective and radiative processes was then found from

$$Q_{\mathrm{total}} = Q_C + \int_{\lambda\,\min}^{\lambda\,\max} \alpha_\lambda Q_{R\lambda}^W\,\mathrm{d}\lambda \tag{8}$$

The contributions of individual radiative processes to the overall radiative transfer were obtained by first solving for the incident radiative flux with all radiative processes intact at each spatial grid location. This information was retained at each grid location, and is displayed as the "total" value in all figures presented. The calculation was then repeated with the contribution of individual processes to the overall emission coefficient (but not the absorption coefficient) deleted in the NEQAIR code and the resulting incident flux retained at each grid point. The difference was then taken between these incident radiative fluxes and the "total" for each case to determine the contribution of individual radiative processes.

In the NEQAIR code, several radiative processes are accounted for. Atomic radiative processes include bound–bound, bound–free, and free–free transitions for both nitrogen and oxygen. Molecular band systems included are the N_2^+ first negative; N_2 first positive, second positive, and Birge–Hopfield bands, NO_β, NO_γ, and O_2 Schumann–Runge. All atomic processes were combined to reflect the contribution of individual species. In earlier work,[15] it was found that bound–bound processes dominated the incident radiative flux resulting from atoms. It was felt that little would be gained by separation of the three modes of atomic radiation, and doing so would incur considerable computational effort. The assumption was made in both the LAURA and NEQAIR codes that vibrational–electronic temperature and the temperature of free electrons are closely coupled, and therefore, the assumption that $T_e = T_V$, where T_e is the temperature of free electrons, was made throughout this study.

LORAN Code

The LORAN code is an approximate nonequilibrium radiation solver. It differs from the NEQAIR code in two principal ways: 1) it employs a "smeared band" model for molecular radiation, to avoid the expense of the line-by-line approach in NEQAIR; 2) it generates an optimized spectrum for the radiation calculation, to minimize the size of the required spectral array. Typical spectral arrays are 3000–5000 spectral points. The details of the development are explained in Refs. 13 and 23. The LORAN code utilizes the same radiative processes as the NEQAIR code, as outlined above.

The motivation for the simplified spectral models was to develop a sufficiently accurate code that would be computationally efficient to allow it to be coupled with the LAURA code. Coupling occurs through the divergence of the radiative flux term that appears in the energy equation. In the LAURA two-temperature approach, the total energy equation contains a flux divergence term containing all radiative effects; the vibrational–electronic energy equation includes radiation effects attributable to vibrational and electronic transitions only. In air, however, the principal transitions of interest involve vibrational and electronic transitions, so the coupling term is the same in both equations in this implementation.

Coupling the two codes has been demonstrated in Ref. 24. The approach that is taken for coupling is based on the experience with equilibrium inviscid [25] and VSL[7] coupled methods. The flowfield is initially converged without the radiation term. Once the initial solution is obtained, radiation is turned on and convergence continues with periodic updates of the radiation. The radiation calculation requires approximately the same amount of CPU time as 2000 iterations of the LAURA code. For this reason, it is desirable to find the largest update interval that will provide efficient convergence. For the nonequilibrium cases typical of the early FIRE II entry, experience has shown that updating radiation every 500 LAURA iterations works well. As equilibrium is approached, radiation is updated less often. In the FIRE II case, the equilibrium flowfields generally have very low radiation, so that coupling effects are minimal in any case.

Radiative transport for the cases in this paper is computed using the tangent slab approximation in LORAN. For comparisons to the radiometer data, the radiative intensity along the stagnation line is computed instead, because the small viewing angle of the radiometer meant that it measured the intensity, not the flux.

Results

The comparisons of the flight data from the FIRE II experiment[3,4] with calculated heat transfer results only use two pieces of actual flight information. The first is the radiative intensity above a wavelength of 2000 Å along the stagnation streamline, obtained from a near-stagnation point radiometer with a quartz window. The second is total heat transfer ($Q_{\mathrm{Total}} = Q_C + \alpha Q_R$), obtained from a total calorimeter in the respective heat shields at a location just off the stagnation point. Therefore, all data presented in this study are for stagnation point heat transfer. Additionally, radiative intensity from 2 to 4 eV was obtained throughout the trajectory, but was not used for this study.

Note that no tabular data were available for the FIRE II experiment, therefore, all flight data presented in this paper were obtained from graphs in Refs. 3 and 4. As with most experimental data, there is some dispersion in the observed values, and the data are subject to some question as to their degree of accuracy. In particular, there is a considerable degree of scatter in the radiative heat transfer data in the early part of the trajectory. The experimental values used for comparison in this study are listed in Table 2. The values were interpreted and/or extrapolated from the graphs in Refs. 3 and 4 by the authors and, as such, are subject to further question because of the inherent inaccuracy in this process. The reader is advised to consult

Table 2 FIRE II extracted data

Time, s	$I(0.2-4.0\mu)$, W/cm^2-sr	Q_{Total}, W/cm^2
1634.0	1.3	175
1636.0	5.2	290
1640.5	35.0	750
1643.0	43.0	1025
1645.0	26.0	1130
1648.0	5.0	730
1651.0	2.8	390
1652.0	1.7	290

the reference materials for their discussion on the accuracy of the experimental data and for interpretation of the data.

No flight data are available on the contributions of individual radiative processes to the overall flux; therefore, all radiative process data are from computational sources alone. Although radiative process data can be calculated from the LORAN code, only data from the NEQAIR code are plotted because few differences other than minor flux magnitude variations were seen between the results from both codes.

FIRE II Calculated Radiative Processes

Analysis of the radiative processes in the FIRE II flowfields was accomplished at four of the selected trajectory points. This analysis was performed, as outlined in the NEQAIR Code section, by use of the uncoupled NEQAIR code. The flux was determined using the thin gas simplification of the flux in Eq. (6). The points chosen for radiative process analysis include the 1634, 1640.5, 1648, and 1652 s trajectory points. In this, and all other sections, trajectory points are referred to by their elapsed time from launch. For the sake of clarity, radiative process figures were plotted using every other flowfield point along the stagnation streamline. The reader should be reminded at this point that it is the incident flux from one gas layer to the next Q_R^{i+1} that is plotted. As such, the flux values constitute a "running total." The radiative flux to the wall is simply the value of Q_R^{i+1} at the wall location.

Figure 3a contains the calculated radiative profiles for the 1634 s case, and Fig. 3b presents the predicted temperature profiles along the stagnation streamline. The flight velocity at this point was 11.36 km/s at an altitude of 76.42 km. Ionization and dissociation were high, as would be expected. Correspondingly, the radiative flux was dominated by atomic nitrogen processes. The initial rapid ionization produces an immediate peak in the atomic nitrogen, which is then quickly self-absorbed. As the vibrational temperature (assumed equal to the electron temperature) begins to peak halfway through the shock layer, the atomic nitrogen flux begins to increase toward a second peak. The atomic nitrogen flux is then absorbed as the flow enters the boundary layer for a radiative contribution of 34 W/cm^2. The other two contributors to the flux at this trajectory point, atomic oxygen and N_2^+ first negative band, have reasonably similar profiles in both their shape and magnitude (approximately 4–5 W/cm^2). Note that there is relatively little absorption in the boundary layer, particularly in the region closest to the wall.

At 1640.5 s (Figs. 3c and 3d) flow velocity is still high (10.97 km/s); however, the flow begins to approach thermal equilibrium at the lower altitude (59.26 km) and higher densities. Comparisons with thermochemical equilibrium codes (not presented here) showed that all flows approached chemical equilibrium as thermal equilibrium was approached. The radiative flux begins to reflect the equilibrium nature of the flowfield, with each gas layer contributing an equal increment to the total flux to the wall, giving the flux plot a linear shape. The flow is almost completely dissociated at this point, and the dominant contributors to the radiative flux are atomic nitrogen and oxygen. Atomic nitrogen is the largest contributor with 504 W/cm^2 to the wall, as opposed to atomic oxygen's 65 W/cm^2. The interior boundary layer absorbs a greater fraction of the flux than the previous case.

In Figs. 3e and 3f (1648 s into the trajectory) ionization begins to fall off at the lower (8.30 km/s) velocity. The N_2 Birge–Hopfield band replaces atomic nitrogen as the primary radiative contributor, although several processes yield roughly similar contributions to the wall radiative flux at this point. The equilibrium nature of the flow is again seen in the linear profile of the radiative flux. The minor absorption in the interior boundary layer is attributable to the increased optical depth for the N_2 Birge–Hopfield band whose spectral region is primarily in the ultraviolet region.

In the final case at 1652 s (Figs. 3g and 3h), the radiative profiles are almost completely linear. The dominant radiator is the NO beta band with 4.3 W/cm^2 at the wall, and NO Gamma and N_2 first positive bands contribute approximately 1.5 W/cm^2 each. At 35.86 km altitude and a velocity of only 5.49 km/s, the flow is in almost complete equilibrium. There is virtually no absorption in the boundary layer for this case.

Coupled and Uncoupled Radiative Heat Transfer

The uncoupled radiative intensities above 2000 Å calculated by the NEQAIR and LORAN codes, as well as the coupled radiative intensity calculated by the LORAN code, are presented with the actual radiometer data from the FIRE II experiment in Fig. 4. This plot shows good comparison by both code results to the radiometer data. The coupled version of LORAN yields radiative intensities well below the observed FIRE II intensities, as well as those calculated in the other methods. Results of both codes tend toward overestimation of the radiative intensity at the early, nonequilibrium points of the FIRE II trajectory, whereas they underestimate the intensity at the lower equilibrium portions of the trajectory. Although the overall trend in this figure shows good agreement, replotting the figure in terms of deviation from flight data reveals serious discrepancies, as shown later.

In Fig. 5a, the calculated radiative flux absorbed by the wall is shown for both codes. Both codes calculated the Q_R using the thin gas estimation of Eq. (6), rather than a tangent slab approximation for this figure. As in the previous figure, the coupled LORAN results are, at the peak heating points, more than 16% below the uncoupled results at the same trajectory points. When this information is viewed in context with the agreement betweeen the two codes in Fig. 4, it implies that almost all disagreement between the two codes comes from their estimation of the flux below 2000 Å wavelength. These differences are only seen at the peak heating points of the trajectory.

In Fig. 5b, the coupled and uncoupled radiative fluxes, calculated by a tangent slab approximation, are plotted. In this comparison, all other flowfield solver parameters and models are held constant; the only difference is the inclusion of radiative flux into the LAURA code's energy equation. Coupling effects reduce the radiative heating rates throughout the trajectory. At the peak radiative heating point, coupling drops the radiative heating by 16%. The tangent slab approximation also lowers the predicted absorbed radiative flux to the wall at all trajectory points, as seen by comparing Figs. 5a and 5b.

Convective and Total Heat Transfer

The effect of coupling the LORAN code to the flowfield solver can be seen in Fig. 6. Convective heating was obtained from the LAURA code, and because the same flowfield solution was used for both the uncoupled NEQAIR and uncoupled LORAN calculations, the convective heat transfer solution does not vary between the two uncoupled results. There was no significant variation in the two profiles with the exception of the 1643 s point of the trajectory; even at this time, the difference between the coupled and uncoupled profiles was only 5%.

A comparison of measured and calculated total heat flux is presented in Figs. 7a and 7b. Figure 7a compares the uncoupled, thin gas predicted values with the measured FIRE II values. The results from both calculations peak approximately 2 s before the measured values. This pattern has been observed by other researchers[5,7] and is independant of the flowfield solution method employed. It is possible, given the number of methods that produce the same pattern (yet, not magnitude) that there was some error in the initial observation of the total heating on the FIRE II vehicle. It is also quite possible that the freestream conditions used at these points are in error. The differences between the total heating calculated by both codes must

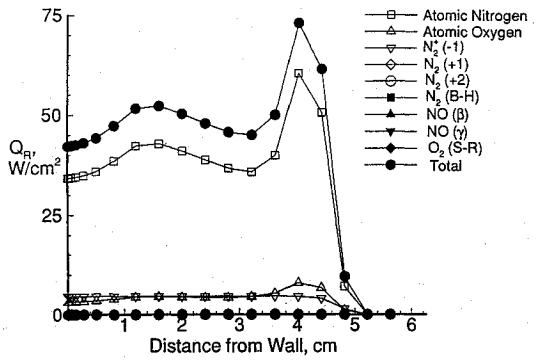

a) 1634 s radiative profile

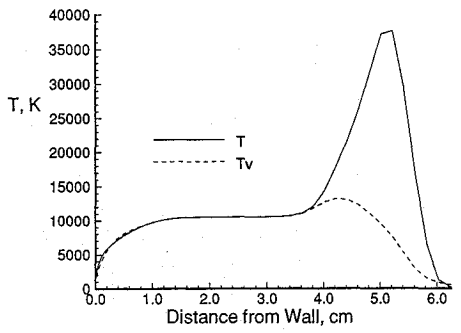

b) 1634 s temperature profile

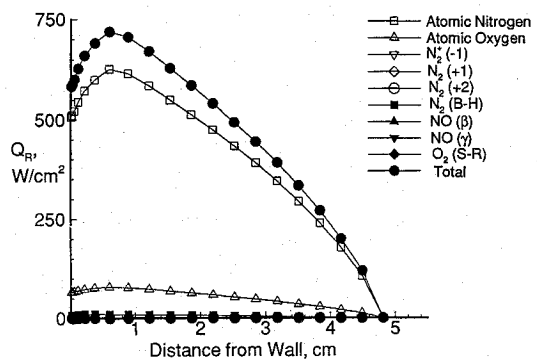

c) 1640.5 s radiative profile

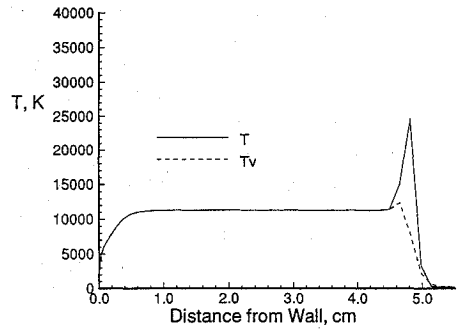

d) 1640.5 s temperature profile

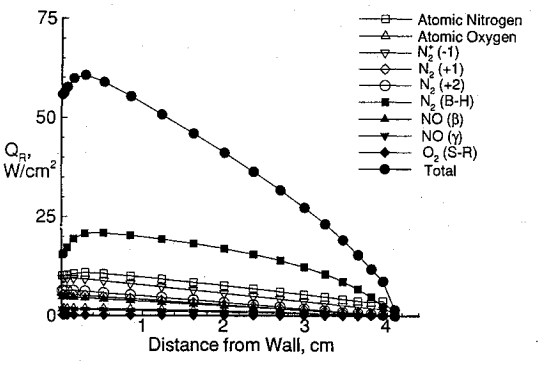

e) 1648 s radiative profile

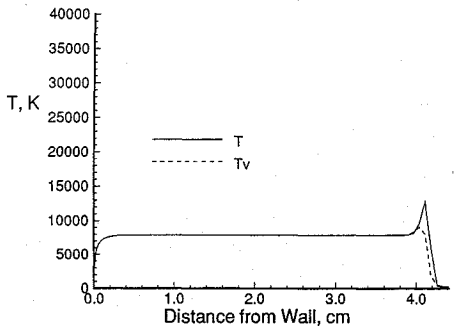

f) 1648 s temperature profile

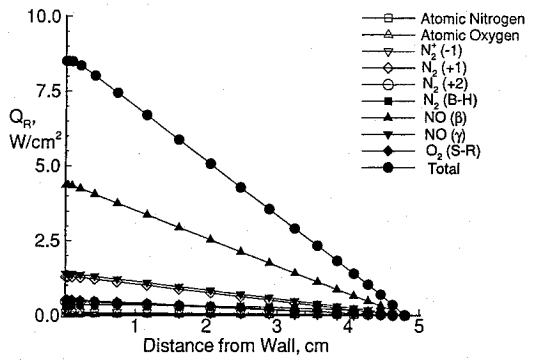

g) 1652 s radiative profile

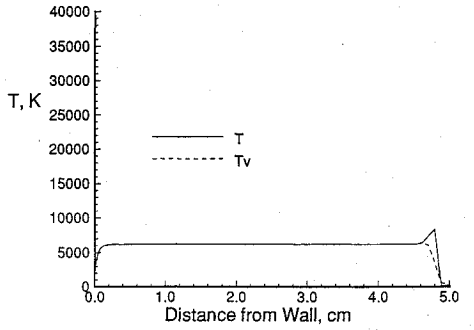

h) 1652 s temperature profile

Fig. 3 Shock layer profiles.

be attributed to the ultraviolet radiative fluxes. Convective heating was identical between the two, by definition. The flux above 2000 Å (Fig. 4) was reasonably similar; the only opportunity for variation is in the calculation of the radiative flux in the spectrum below 2000 Å.

Figure 7b presents the coupled total heating. In the early part of the FIRE II trajectory, coupling effects reduce the radiative heating rates by 4–8%. At 1643 s (the peak predicted heating point and also the peak radiative heating point), coupling decreases the radiative heating 16%, but increases the convective flux by 6% in opposition to the trend early in the trajectory. The net effect is only a 2% decrease in the total heat flux to the surface. At the peak experimental heating point (1645 s), the coupling is less, and its effect cancels completely between the decrease in radiative flux and the increase in convective flux. The coupling effect decreases to only a few percent as the vehicle continues to slow down in the lower atmosphere. At 1651 s and beyond, the radiative effects are so small that no coupling effect occurs. In general, coupling effects are quite small for the entire FIRE II trajectory.

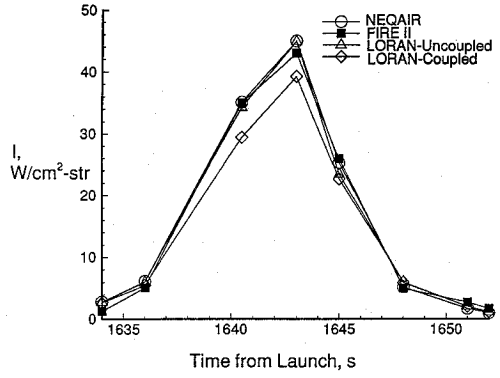

Fig. 4 Comparison of stagnation radiative intensity, 2000–15,000 Å.

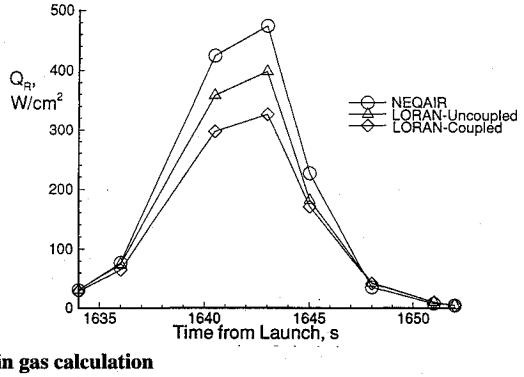

a) Thin gas calculation

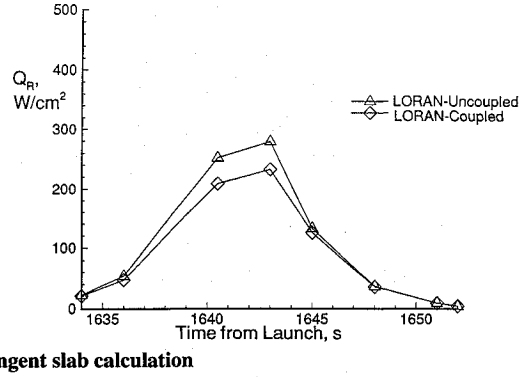

b) Tangent slab calculation

Fig. 5 Total absorbed radiative flux αQ_R.

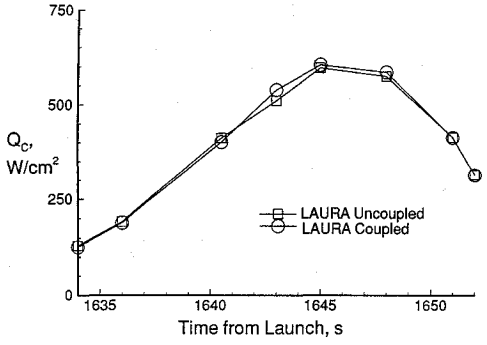

Fig. 6 Convective heating Q_C.

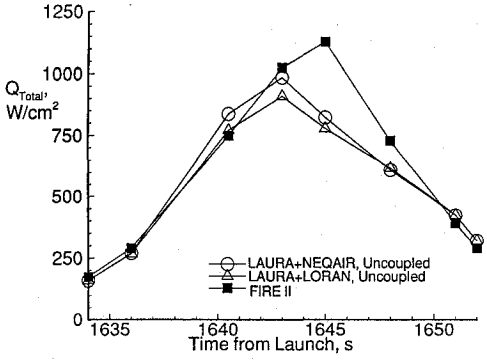

a) Thin gas calculation

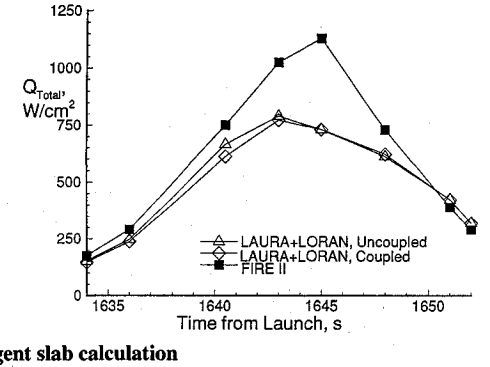

b) Tangent slab calculation

Fig. 7 Total heat transfer $Q_C + \alpha Q_R$.

Discussion

The present study produced many unexpected results as well as results that are subject to interpretation. Although Fig. 4 would allow the conclusion that the uncoupled radiative transfer codes produce excellent agreement with the measured radiative intensities for the FIRE II vehicle, the same results, when plotted as a percentage deviation from the FIRE II values, as in Fig. 8a, give a different conclusion. All versions of the nonequilibrium radiative heat transfer calculation methods, coupled or uncoupled, overestimate the radiative intensities at the most nonequilibrium point (1634 s) by more than 100%. This region is precisely where the greatest accuracy from a nonequilibrium method would be expected. After the 1634 s point, the margin of error became ±30%. The same codes tend to underestimate the radiative intensity at the highly equilibrium points of 1651–1652 s. In contrast, previous equilibrium calculations[5] were within ±30% from 1631 s on. Because all nonequilibrium results share a common flowfield solver, the LAURA code, it is possible that there is some thermodynamic quantity that is incorrectly calculated, or some incorrectly based nonequilibrium model in the LAURA code.

The profiles in Fig. 8a show a trend from overestimation, to reasonable accuracy, to underestimation. This gives the intuitive impression of an inappropriate curve fit within either the LAURA code or within the radiation codes, because they also share certain rate constants. However, as stated earlier, this is subject to interpretation. When the overall heat transfer is compared to the radiative heat transfer, it can be shown that the radiative portion is minimal at the trajectory points experiencing the greatest deviation from observed values. Therefore, all radiative heat transfer codes yield good results at the trajectory points where radiative heat transfer contributes the most to the total heating for the FIRE II. This may not be the case for other vehicles following different trajectories, and suggests that more fundamental research is needed on nonequilibrium modeling.

Figure 8b plots the variation from observed FIRE II of the total heat transfer. Given the computational margin of error for both the convective and radiative heat calculations, and the fact that these will compound when combined in a uncoupled fashion, the agreement between calculated values and observed values is fairly good. It was noted earlier in this study that the LORAN code tends to underestimate the ultraviolet radiative flux, and this is demonstrated here in the early portion of the FIRE II trajectory, while all codes tend to produce identical variations of total heating as equilibrium is approached.

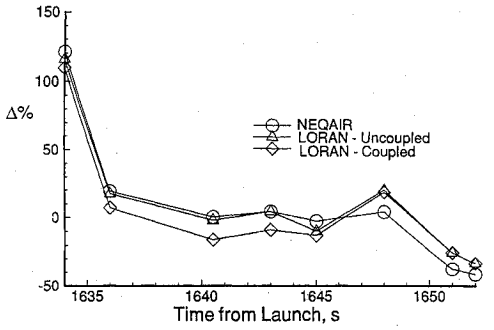

a) Variation in radiative intensity from FIRE II, 2,000–15,000 Å

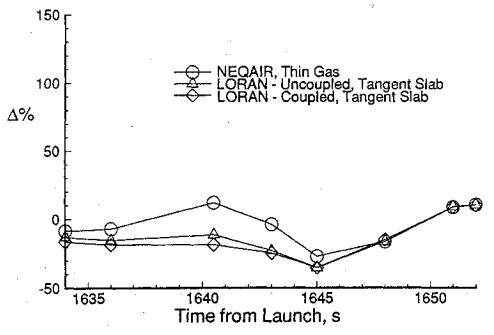

b) Variation in total heating from FIRE II

Fig. 8 Percent variation of calculated data from FIRE II experiment.

Concluding Remarks

One disturbing conclusion that can be made from the preceding study is that the nonequilibrium flowfield and radiation solution methods of the present research yield no better agreement in the nonequilibrium portions of the trajectory than do the simpler methods of past studies. The current solution methods do converge toward good agreement as equilibrium conditions are approached, and the LAURA, NEQAIR, and LORAN codes yield good results at those trajectory points. However, nonequilibrium models require further research and modifications in both the convective and radiative heating calculations; albeit that nonequilibrium radiative methods require the most study. We should not get the impression from the present research that this is an insignificant problem. The disagreement between measured and calculated heating values for the FIRE II vehicle was the greatest where total heat transfer was minor compared to the heat transfer at lower altitude trajectory points. Heat shields of future vehicles would be designed for the peak heating point. However, the FIRE II trajectory will not be followed by all future vehicles, and aerobrake vehicles may only encounter flow regimes similar to the early portion of the FIRE II's trajectory where the disagreement between measured and computed values was the greatest. This would pose a challenge in the correct design of such vehicles heat shields.

One final observation must be made. It is usually assumed that in the high energy flows encountered by the FIRE II vehicle, coupling of the radiative heat transfer to the energy equation is necessary for the correct estimation of the overall heating. Although coupling represents a more advanced degree of computational accuracy, and coupled results produced similar profiles to the uncoupled results, the coupled results were approximately 20% below the experimental profiles. It is expected that coupling, by lowering the temperatures in the shock layer through radiative cooling, would produce a reduced value of radiative heat transfer. It is possible, then, that all radiative models are inherently understating radiative flux values in the peak heating portion of the trajectory, and the agreement between the magnitude of the uncoupled calculated fluxes and the experimental results at peak heating is fortuitous. Remember that the nonequilibrium physical models used in LAURA and NEQAIR were generally developed without coupling effects.

Acknowledgments

The preceding study was sponsored in part by NASA Contract NAS1-19237. The authors thank their technical monitor, David Throckmorton, for his support.

References

[1]Lee, D. B., and Goodrich, W. D., "The Aerothermodynamic Environment of the Apollo Command Module during Superorbital Entry," NASA TN D-6792, 1972.

[2]Seiff, A., Reese, D. E., Sommer, S. C., Kirk, D. B., Whiting, E. E., and Niemann, H. B., "PAET, An Entry Probe Experiment in the Earth's Atmosphere," *Icarus*, Vol. 18, 1973, pp. 525–563.

[3]Cornette, E. S., "Forebody Temperatures and Calorimeter Heating Rates Measured During Project FIRE II Reentry at 11.35 Kilometers per Second," NASA TM X-1305, Nov. 1966.

[4]Cauchon, D. L., "Radiative Heating Results from the FIRE II Flight Experiment at a Reentry Velocity of 11.4 Kilometers per Second," NASA TM X-1402, July 1967.

[5]Sutton, K., "Air Radiation Revisited," AIAA Paper 84-1733, June 1984.

[6]Balakrishnan, A., Park, C., and Green, M. J., "Radiative Viscous Shock Layer Analysis of Fire, Apollo, and PAET Flight Data," AIAA Paper 85-1064, June 1985.

[7]Gupta, R. N., "Navier–Stokes and Viscous Shock-Layer Solutions for Radiating Hypersonic Flows," AIAA Paper 87-1576, June 1987.

[8]Park, C., "Assessment of Two-Temperature Kinetic Model for Ionizing Air," AIAA Paper 87-1574, June 1987.

[9]Hartung, L. C., Mitcheltree, R. A., and Gnoffo, P. A., "Stagnation Point Nonequilibrium Radiative Heating and the Influence of Energy Exchange Models," AIAA Paper 91-0571, Jan. 1991.

[10]Gnoffo, P. A., "Upwind-Biased, Point-Implicit Relaxation Strategies for Viscous, Hypersonic Flows," AIAA Paper 89-1972, June 1989.

[11]Gnoffo, P. A., Gupta, R. N., and Shinn, J., "Conservation Equations and Physical Models for Hypersonic Air Flows in Thermal and Chemical Nonequilibrium," NASA TP 2867, Feb. 1989.

[12]Park, C., "Nonequilibrium Air Radiation (NEQAIR) Program: User's Manual," NASA TM 86707, July 1985.

[13]Hartung, L. C., "Development of a Nonequilibrium Radiative Heating Prediction Method for Coupled Flowfield Solutions," *Journal of Thermophysics and Heat Transfer*, Vol. 6, No. 4, 1992, pp. 618–625.

[14]Gnoffo, P. A., Hartung, L. C., and Greendyke, R. B., "Heating Analysis for a Lunar Transfer Vehicle at Near-Equilibrium Flow Conditions," AIAA Paper 93-0270, Jan. 1993.

[15]Greendyke, R. B., "Parametric Analysis of Radiative Structure in Aerobrake Shock Layers," *Journal of Spacecraft and Rockets*, Vol. 30, No. 1, 1993, pp. 51–58.

[16]Roe, P. L., "Approximate Riemann Solvers, Parameter Vectors, and Difference Schemes," *Journal of Computational Physics*, Vol. 43, No. 2, 1981, pp. 357–372.

[17]Harten, A., "High Resolution Schemes for Hyperbolic Conservation Laws," *Journal of Computational Physics*, Vol. 49, No. 3, 1983, pp. 357–393.

[18]Weilmuenster, K. J., and Gnoffo, P. A., "Solution Strategies and Heat Transfer Calculations for Three-Dimensional Configurations at Hypersonic Speeds," AIAA Paper 92-2921, July 1992.

[19]Greendyke, R. B., Gnoffo, P. A., and Lawrence, R. W., "Electron Number Density Profiles for the Aeroassist Flight Experiment," AIAA Paper 92-0804, Jan. 1992.

[20]Park, C., *Nonequilibrium Hypersonic Aerothermodynamics*, Wiley, New York, 1990, pp. 255–280.

[21]Hansen, C. F., "Collision-Induced Gas Phase Dissociation Rates," Final Rept., NASA Grant NAG1-1046, Aug. 1990.

[22]Arnold, J. O., Whiting, E. E., and Lyle, G. C., "Line By Line Calculation of Spectra from Diatomic Molecules and Atoms Assuming A Voight Line Profile," *Journal of Quantitative Spectroscopy & Radiative Transfer*, Vol. 9, No. 6, 1969, pp. 775–798.

[23]Hartung, L. C., "Nonequilibrium Radiative Heating Prediction Method for Aeroassist Flowfields with Coupling to Flowfield Solvers," Ph.D. Dissertation, North Carolina State Univ., 1991.

[24]Hartung, L. C., Mitcheltree, R. A., and Gnoffo, P. A., "Coupled Radiation Effects in Thermochemical Nonequilibrium Shock-Capturing Flowfield Calculations," AIAA Paper 92-2868, July 1992.

[25]Sutton, K., "Characteristics of Coupled Nongray Radiating Gas Flows with Ablation Products Effects About Blunt Bodies During Planetary Entries," Ph.D. Dissertation, North Carolina State Univ., 1973.